Loss of nodal quasiparticle integrity in underdoped YBa$_2$Cu$_3$O$_{6+x}$

D. Fournier,[1] G. Levy,[1] Y. Pennec,[1] J.L. McChesney,[2] A. Bostwick,[2] E. Rotenberg,[2]
R. Liang,[3] W.N. Hardy,[1,3] D.A. Bonn,[1,3] I.S. Elfimov,[3] and A. Damascelli[1,3]

[1]*Department of Physics & Astronomy, University of British Columbia, Vancouver, British Columbia V6T 1Z1, Canada*
[2]*Advanced Light Source, Lawrence Berkeley National Laboratory, Berkeley, California 94720, USA*
[3]*AMPEL, University of British Columbia, Vancouver, British Columbia V6T 1Z4, Canada*

Arguably the most intriguing aspect of the physics of cuprates is the close proximity between the record high-T_c superconductivity (HTSC) and the antiferromagnetic charge-transfer insulating state driven by Mott-like electron correlations. These are responsible for the intimate connection between high and low-energy scale physics [1–3], and their key role in the mechanism of HTSC was conjectured very early on [4]. More recently, the detection of quantum oscillations in high-magnetic field experiments on YBa$_2$Cu$_3$O$_{6+x}$ (YBCO) has suggested the existence of a Fermi surface of well-defined quasiparticles in underdoped cuprates [5, 6], lending support to the alternative proposal that HTSC might emerge from a Fermi liquid across the whole cuprate phase diagram [7, 8]. Discriminating between these orthogonal scenarios hinges on the quantitative determination of the elusive quasiparticle weight Z, over a wide range of hole-doping p. By means of angle-resolved photoemission spectroscopy (ARPES) on in situ doped YBCO [9], and following the evolution of bilayer band-splitting, we show that the overdoped metal electronic structure ($0.25 \lesssim p \lesssim 0.37$) is in remarkable agreement with density functional theory [10–12] and the $Z = 2p/(p+1)$ mean-field prediction [13, 14]. Below $p \simeq 0.10$-0.15, we observe the vanishing of the nodal quasiparticle weight Z_N; this marks a clear departure from Fermi liquid behaviour and – consistent with dynamical mean-field theory [15] – is even a more rapid crossover to the Mott physics than expected for the doped resonating valence bond (RVB) spin liquid [13, 14].

Formally, the degree of quasiparticle integrity is revealed by $Z_k \equiv \int A_{coh}(k, \omega)\,d\omega$, i.e. the integrated spectral weight of the coherent part of the single-particle spectral function $A(k, \omega) \equiv A_{coh}(k, \omega) + A_{incoh}(k, \omega)$ probed by ARPES [16, 17]. Experimentally, while in the optimally-to-overdoped regime Z_k is believed to be finite – yet quantitatively undetermined – at all momenta both above and below T_c, the situation is much more controversial in the optimally-to-underdoped regime [16, 17]. Although it has been conjectured that the $T = 0$ extrapolation of the pseudogap state is a nodal (N) liquid [18, 19], a determination of Z_N has not been possible. As for the antinodal (AN) quasiparticle spectral weight,

the ARPES spectra are characterized by a dramatic temperature dependence, with broad incoherent features in the pseudogap state and quasiparticle-like excitations emerging below T_c [16, 17]; this observation led to the early proposal that the onset of HTSC might be thought of as a 'coherence transition' [20]. Detailed doping-dependent studies reported a decreasing Z_{AN} upon reducing p [21, 22]; however, whether $Z_{AN} \propto p$ [22] or vanishes at finite p [21] remains unresolved, because of the experimental difficulty in the quantitative discrimination between A_{coh} and A_{incoh}. As discussed in greater detail in the Supplementary Information, where we present an analysis of the quasiparticle spectral weight across the whole YBCO phase diagram, this is particularly challenging on the underdoped side where Z_k vanishes; and even in the overdoped regime, this allows at best a relative – rather than absolute – determination of Z_k.

As an alternative, potentially more quantitative approach, in materials with CuO$_2$ bilayers within the unit cell such as Bi$_2$Sr$_2$CaCu$_2$O$_{8+\delta}$ (Bi2212) and YBCO, the quasiparticle strength Z_k might be estimated from the bonding (B) and antibonding (AB) band splitting $\epsilon^{B,AB}(k) = \epsilon(k) \mp t_\perp(k)$, where $\epsilon(k)$ is the quasiparticle dispersion with respect to the in-plane momentum k, and $t_\perp(k)$ accounts for the interplane coupling. Access to Z_k is provided by the fact that both $\epsilon(k)$ and $t_\perp(k)$, as measured by ARPES, correspond to *effective* quantities; under the assumption that correlation effects renormalize the bandwidth but *not* the functional form of the quasiparticle dispersion, these effective quantities are related to the *density functional theory* values through the same renormalized quasiparticle strength Z_k. This assumption is most appropriate along the nodal direction of cuprates [16, 17], which is the focus of our study since *nodal quasiparticles* – being unaffected by the opening of pseudo and superconducting gaps – provide access to the normal state underlying the emergence of HTSC. This approach for the extraction of Z_k will be experimentally validated based on a direct comparison with results for the quasiparticle spectral weight.

The renormalization of the in-plane hopping probability due to correlations is given by the ratio between the number of ways an electron can be added to the Mott-like system as compared to the independent particle system. While in the latter this is proportional to the total number $1 + p$ of available band states [1 at half-filling ($p = 0$), and 2 for a completely empty band ($p = 1$)], in the Mott-
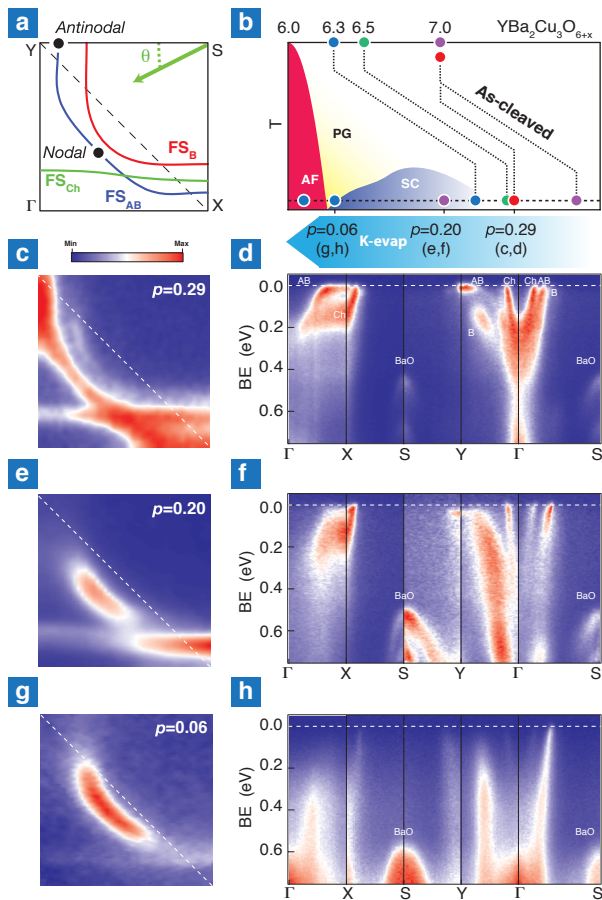
FIG. 1: **Fermi surface and band dispersion across the YBCO phase diagram**. (a) Schematics of the Fermi surface of optimally doped YBCO from band-structure calculations: three sheets of Fermi surface (FS_{Ch}, FS_B, FS_{AB}) are derived from the one-dimensional CuO-chain (Ch) band, and the bonding (B) and antibonding (AB) CuO$_2$-plane bands. (b) YBCO doping-range for bulk (oxygen content, top axis) and surface (hole-doping p, bottom axis) investigated in this work. Color dots refer to different samples of various oxygen content; from the combination of as-cleaved and K-deposited surfaces, a doping p ranging from 0.37 to 0.02 could be accessed. (c-h) Fermi surface and band dispersion, as determined by ARPES at $T = 20$ K, for three representative hole-doping levels obtained on: self-doped as-cleaved YBCO7 [(c,d), $p = 0.29$, red dot in b], a second K-evaporated YBCO7 sample [(e,f), $p = 0.20$, purple dot in b], and heavily K-evaporated YBCO6.3 [(g,h), $p = 0.06$, blue dot in b]. At $T = 20$ K the data are representative of the overdoped normal metal (c, large FS_B FS_{AB} barrels), the nearly optimally doped superconductor (e, gapped Fermi surface with nodal Dirac points), and the underdoped pseudogap state (g, Fermi arcs).

correlated case it is proportional to the doping p away from half-filling, times a factor of 2 because for each hole induced by doping an electron can be added with spin up or spin down [1]. This leads to the mean-field result

$Z = 2p/(p+1)$ [13, 14], and is the same for in-plane and interplane hopping since both processes are governed by the same correlation effects. The effective bilayer splitting can be written as $\Delta\epsilon_k^{B,AB} = 2t_\perp(k) = 2Z_k t_\perp^{LDA}(k)$; its detection by ARPES and the a-priori knowledge of $t_\perp^{LDA}(k)$, as derived from local-density approximation (LDA) band structure calculations, allows a quantitative determination of Z_k.

A study of this kind has been performed on Bi2212 at the antinodes in the optimal-to-overdoped regime [23]; however, a systematic investigation in the underdoped regime is lacking. A potentially more promising candidate for such a study of Z_k is YBCO, which is characterized by a larger bilayer splitting especially along the nodal direction [10–12]; furthermore, although YBCO has long been considered unsuitable for ARPES because of the polar-catastrophe-driven overdoping of the cleaved surface [9, 12], the in situ doping method based on the deposition of potassium allows exploration of a doping range much wider than for any other cuprate family [9]. Here we apply this approach to detwinned YBa$_2$Cu$_3$O$_{6+x}$ single crystals for several values of the bulk oxygen content: $(6+x) = 6.34$, 6.35, 6.51, and 6.99 (hereafter referred to as YBCO6.3, YBCO6.5, and YBCO7). As summarized in the YBCO phase diagram of Fig. 1b, by performing ARPES on different as-cleaved and K-deposited samples we can follow the evolution of the electronic structure from the heavily overdoped ($p \simeq 0.37$, by far the highest among all overdoped cuprates including Tl$_2$Ba$_2$CuO$_{6+\delta}$ [24]), to the deeply underdoped regime ($p \simeq 0.02$).

In the overdoped regime ($p = 0.29$, Fig. 1c), we observe three Fermi surfaces (FS_{Ch}, FS_B, FS_{AB}), in agreement with LDA band-structure calculations (Fig. 1a). These correspond to the one-dimensional CuO-chain (Ch) band, and the B and AB CuO$_2$-plane bands. The dispersions of the bands seen by ARPES (Fig. 1d) are also consistent with the LDA results, with the exception of the BaO band that in the calculations is located at the Fermi energy [10, 11], but in the experiment is found at ~ 450 meV binding energy (similar disagreement is encountered for TlO [24] and BiO bands [25] in Tl- and Bi-cuprates). Upon reaching the underdoped regime by potassium deposition on the as-cleaved surfaces, behaviour consistent with the established phenomenology of underdoped cuprates is seen [18, 26–29]; the CuO$_2$-plane Fermi surface barrels become partially gapped and reduce to four nodal 'Dirac points' (somewhat broadened by resolution) in the $p = 0.20$ superconductor (Fig. 1e), and to four extended Fermi arcs in the $p = 0.06$ pseudogap phase (Fig. 1g). The spectral function becomes progressively more incoherent, with reduced low-energy quasiparticle intensity and a continuum of spectral weight extending to increasingly higher binding energy (Fig. 1f,h). We also observe a progressive change in FS_{Ch} volume and BaO binding energy (Fig. 1c-h); as discussed in the Supplementary Information, monitoring the evolution of these
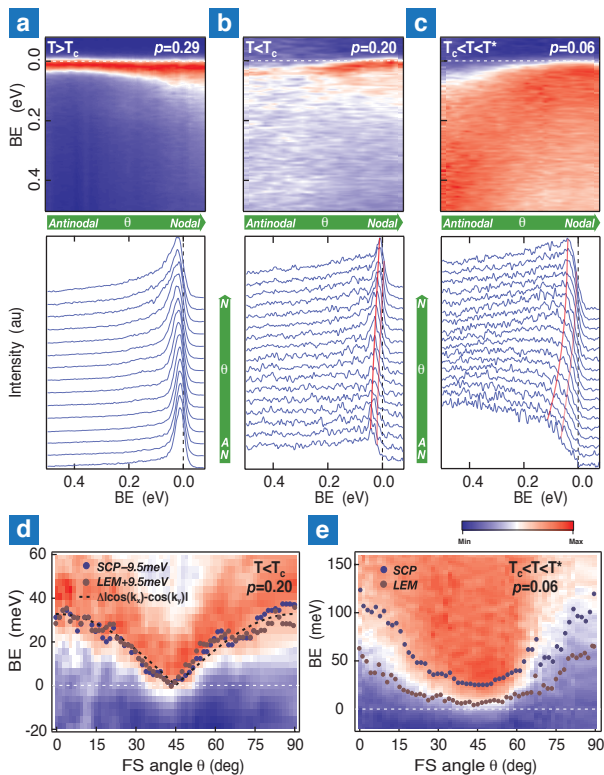
FIG. 2: **Doping evolution of the gap in YBCO**. (a-c) ARPES image plots and selected energy distribution curves (EDCs), from the antinodal to the nodal region, along the AB-band Fermi surface and minimum gap contour. The data were obtained at $T = 20\,\mathrm{K}$ on the same three samples of Fig. 1: (a) overdoped normal metal ($p = 0.29$, $T > T_c$); (b) nearly-optimally doped superconductor ($p = 0.20$, $T < T_c$); (c) underdoped pseudogap state ($p = 0.06$, $T_c < T < T^*$). While gapless metallic behavior is observed for $p = 0.29$ (a), a v-shape gap consistent with the d-wave functional form is detected for $p = 0.20$ (d), as evidenced by the evolution of both superconducting peak (SCP) and leading-edge midpoint (LEM) as a function of the Fermi surface angle θ defined in Fig. 1a. For $p = 0.06$ (e), a much more rounded gap profile is observed, consistent with the established pseudogap and Fermi arc phenomenology (in this latter case SCP corresponds to the minima in the second energy derivative of the EDCs).

features allows the precise determination of the effective surface hole-doping p induced by potassium deposition.

As for the superconductivity related features, Fig. 2 shows image plots and selected energy distribution curves (EDCs) from the antinodal to the nodal region, along the AB-band Fermi surface and minimum gap contour. The $p = 0.29$ EDCs have no marked momentum dependence, typical of metallic behavior (Fig. 2a). At $p = 0.20$ (Fig. 2b and d), a clear v-shape gap consistent with the $d_{x^2-y^2}$ HTSC gap is evidenced by the momentum evolution of both leading-edge midpoint (LEM) and superconducting peak (SCP). The $\Delta|\cos(k_x) - \cos(k_y)|$ fit of the average

of the two (Fig. 2d) returns a maximum antinodal gap value $\Delta \simeq 34\,\mathrm{meV}$, consistent with the $2\Delta \sim 70\,\mathrm{meV}$ reported for HTSCs with $T_c^{max} \sim 95\,\mathrm{K}$ [29]; this also gives $v_F/v_2 = 15 \pm 1$, where v_2 is the slope of the gap at the node and $v_F = 1.42 \pm 0.05\,\mathrm{eV\mathring{A}}$. At $p = 0.06$, the quasiparticle peaks and d-wave-like superconducting gap are replaced by broad incoherent features with marginally defined LEM and SCP (Fig. 2c); these describe a rounded pseudo-gap-like profile [27], with a much larger Δ at the antinodes (Fig. 2e). This behavior, and the associated Fermi arc phenomenology (Fig. 1g), are hallmarks of the pseudogap phase [18, 26–29].

The ($T = 20\,\mathrm{K}$) results in Fig. 1 and 2 reproduce the major features of the cuprate electronic structure in the overdoped normal metal ($p = 0.29$, $T > T_c$), the nearly-optimally doped superconductor ($p = 0.20$, $T < T_c$), and the underdoped pseudogap state ($p = 0.06$, $T_c < T < T^*$). Most importantly, they demonstrate that in situ potassium doping of cleaved YBCO provides a very effective means of exploring the whole cuprate phase diagram via surface-sensitive single-particle spectroscopies. We will now discuss the evolution of k_F and B-AB bilayer band splitting along the nodal direction, aiming at a quantitative determination of Z_k. As shown in Fig. 3a for YBCO6.3, the B and AB bands are clearly resolved in the overdoped regime ($p = 0.24$), while only one dispersive feature is detected at low doping values ($p = 0.06$); a similar evolution has been observed on all YBCO samples. By fitting the momentum distribution curves (MDCs) at E_F with Lorentzian lineshapes convoluted with a Gaussian to account for the instrumental resolution (Fig. 3a,b), we extract $k_{F,N}$ from $p = 0.37$ all the way to 0.02. Bilayer splitting is progressively reduced upon underdoping and below $p \simeq 0.15$ only one CuO_2 band is detected (Fig. 3c). From the linear fit of B and AB nodal $k_{F,N}$ versus doping we identify a vanishing $p_c = 0.12 \pm 0.02$, consistent with the recent interpretation of optical – and thus bulk sensitive – data from YBCO, which also suggest the suppression of bilayer splitting between 6.5 and 6.75 oxygen content [30].

As for the evolution of Z_k, we start from the heavily overdoped regime ($p > 0.25$, region III in Fig. 3c), where ARPES is in overall quantitative agreement with the LDA calculations. At $p = 0.37$ (i.e., overdoped normal metal), we can accurately determine both the N and AN bilayer splittings, $\Delta\epsilon_N^{B,AB} = 130 \pm 10\,\mathrm{meV}$ and $\Delta\epsilon_{AN}^{B,AB} = 150 \pm 10\,\mathrm{meV}$. From the LDA values $t_\perp^{LDA}(N) \simeq 120\,\mathrm{meV}$ and $t_\perp^{LDA}(AN) \simeq 150\,\mathrm{meV}$ (Supplementary Information), and making use of the relation $\Delta\epsilon_k^{B,AB} = 2Z_k t_\perp^{LDA}(k)$, we obtain $Z_N \simeq 0.54$ and $Z_{AN} \simeq 0.50$. Upon underdoping, we focus on the nodal direction where the bilayer splitting can be detected both as $\Delta k_{F,N}^{B,AB}$ and $\Delta\epsilon_N^{B,AB}$, owing to the presence of the gap nodes. While the results in region II are still at least qualitatively consistent with LDA ($0.12 < p < 0.25$), the dis-
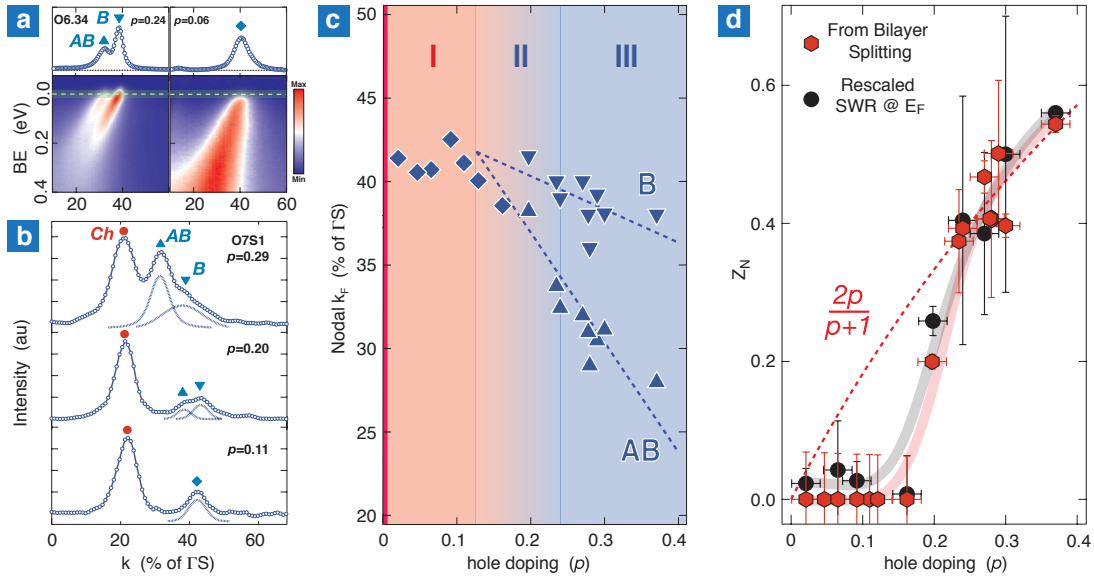
FIG. 3: **Doping evolution of nodal $k_{F,N}^{B}$, $k_{F,N}^{AB}$, and Z_N.** (a) ARPES nodal dispersion and corresponding E_F momentum distribution curves (MDCs; ± 15meV integration, see shaded region), from as-cleaved and K-deposited YBCO6.34, for light polarization parallel to Γ-S. (b) Similar MDCs from YBCO7, for light polarization parallel to Γ-Y (note the polarization-dependent change of Ch, B, and AB intensity). (c) Evolution of $k_{F,N}^{B}$ (down triangles) and $k_{F,N}^{AB}$ (up triangles) along the nodal direction (distance from the Γ point in percentage of Γ-S), as determined by ARPES across the entire hole-doping phase diagram of YBCO; below $p \simeq 0.15$ the bilayer B-AB splitting vanishes and only one single $k_{F,N}$ is detected (diamonds). (d) Nodal quasiparticle renormalization Z_N as determined from the observed bilayer splitting ($Z_N = \Delta\epsilon_N^{B,AB}/2t_\perp^{LDA}(N)$ with $t_\perp^{LDA}(N) \simeq 120$ meV) and the low-energy spectral-weight ratio (SWR) defined as $\int_{E_F}^{-\infty} I(k_{F,N},\omega)\,d\omega / \int_{0.8\,eV}^{-\infty} I(k_{F,N},\omega)\,d\omega$ from the ARPES intensity $I(k,\omega) = I_0(k)f(\omega)A(k,\omega)$. The SWR was rescaled so that the two curves match in the $0.23-0.37$ doping range (see Supplementary Information). Thick gray and orange lines are spline guides to the eye, while the dashed red line is the mean-field relation $2p/(p+1)$ [13, 14]. For the bilayer splitting data, the error bars are defined from the B-AB MDC fits when bilayer splitting is detected, and from the experimental resolutions otherwise; for the SWR data, they are calculated from the spread in the SWR values for integration windows smaller than $[0.1\,eV, -\infty]$ (Fig. 3 in Supplementary Information).

appearance of bilayer splitting in the underdoped regime ($p < 0.12$, region I in Fig. 3c) marks a clear departure from the independent-particle description. Note that LDA would give a nearly doping-independent $\Delta k_{F,N}^{B,AB}$ with $(k_{F,N}^{AB};\ k_{F,N}^{B}) = (33.0;38.7), (35.2;39.5)$, and $(38.0;42.2)$ for O7.0, O6.5, and O6.0, respectively [11]. Furthermore, the value of bilayer splitting is also rather insensitive to electrostatic effects associated with the presence of different concentrations of O^{2-} ions in the CuO chain layers or K^{1+} above the BaO terminations, due to the vanishing potential these charged layers exert on the CuO$_2$ bilayer (Supplementary Information).

The bilayer-splitting-derived results for Z_N across the whole phase diagram are presented in Fig. 3d, together with the nodal spectral-weight ratio (SWR) estimated at E_F (see caption for definition). When calculated for integration windows smaller than $[0.1\,eV, -\infty]$ in binding energy, the SWR provides a relative measure of the degree of quasiparticle integrity Z_N (Supplementary Information). Although not a quantitative estimate of Z_N, the doping evolution of the low-energy SWR is reminiscent of the quasiparticle renormalization inferred from the bilayer splitting. When the two results are plot-

ted together (after the necessary rescaling of the SWR, so that the two curves match in the $0.23-0.37$ doping range), the similarity is striking (Fig. 3d), validating the quantitative determination of Z_N from the evolution of bilayer band splitting. Furthermore, the agreement with the $2p/(p+1)$ relation above $p \simeq 0.23$ provides an unprecedented quantitative estimate of quasiparticle integrity in overdoped cuprates, which supports a description of the normal-state electronic structure based on density functional theory with nearly isotropic quasiparticle renormalization factors, as in the spirit of Fermi liquid theory. Below $p \simeq 0.23$, however, Z_N deviates from $2p/(p+1)$, vanishing in the $p \simeq 0.10 - 0.15$ range where the error bars in Fig. 3d define an upper limit $Z \simeq 0.065$. From this we can estimate a corresponding upper limit for the nodal bilayer splitting $\Delta\epsilon_N^{B,AB} \simeq 15.6$ meV, which is consistent with the value of 8 meV reported based on the analysis of quantum oscillation results [31, 32]. Note also that in region I, not only have the bilayer splitting and Z_N vanished, the doping evolution of $k_{F,N}$ appears to have saturated, despite the fact that the CuO$_2$ planes are still becoming more underdoped as evidenced by the further increase of pseudogap magnitude and high-energy

incoherent spectral weight. This indicates that, upon approaching the charge-transfer insulator, the quasiparticle integrity is lost even faster than hinted by renormalized mean-field treatments of the doped spin liquid [13, 14]. It also suggests that the emergence of the Mott physics in cuprates might be captured by cluster dynamical mean-field theory calculations, which predict a similarly rapid suppression of Z_N in the $p \simeq 0.10$–0.15 doping range [15].

Finally, we note that a vanishing Z_N does not imply vanishing of the total single-particle spectral weight, but rather a redistribution from coherent to incoherent components of $A(k,\omega)$. While for $p = 0.06$ we find $Z_N \simeq 0$, spectral weight is still present all the way to E_F (Fig. 3a and Supplementary Information); however, the distinction between A_{coh} and A_{incoh} is becoming completely blurred. This suggests something similar to early exact diagonalization cluster calculations for Mott-Hubbard and charge-transfer models [1], where it is the *total* and not just the *coherent* spectral weight that vanishes as $2p/(p+1)$. Indeed, optical spectroscopy [33] shows that the total low-frequency ($\omega \lesssim 75$ meV) integrated spectral weight – whether associated with a well defined Drude peak or an incoherent band – scales to zero with the doping p [33]. More fundamentally, the loss of quasiparticle integrity implies the breakdown of concepts such as Fermi surface, band dispersion and Fermi velocity, as well as Luttinger's sum rule, and suggests that below $p \lesssim 0.10 - 0.15$ the physical properties of underdoped cuprates (in zero-field) are dominated by incoherent excitations.

METHODS

Sample preparation. For this study we used detwinned $YBa_2Cu_3O_{6+x}$ single crystals with $x = 0.34$, 0.35, 0.51, and 0.99 (see Ref. 9 for details on growth, annealing, and detwinning procedures).
ARPES experiments. ARPES measurements were performed at Beamline 7.01 of the Advanced Light Source, with linearly-polarized 100 and 110 eV photons and a Scienta-R4000 electron analyzer ($\Delta E \simeq 30$ meV and $\Delta\theta \simeq 0.1°$). The light polarization was parallel to the plane of emission, while the samples were aligned with the in-plane Cu-O bonds either parallel or at 45° with respect to the polarization (resulting in more intensity for the antinodal/chain or nodal features, respectively). Fermi surface maps were obtained by integrating the ARPES intensity over a 30 meV energy window about E_F, and then normalized relative to one another for display purposes. Mounted on a 5-axis manipulator, the samples were cleaved at 20 K and 2.5×10^{-11} torr, and oriented in situ by taking fast Fermi surface scans.

The self-doping of the YBCO surfaces for various bulk oxygen contents was tuned towards the underdoped regime by in situ deposition of submonolayers of potassium. We acquired data on the as-cleaved surfaces, as well as after subsequent potassium evaporations from a commercial SAES alkali-metal dispenser; evaporation current and time were precisely monitored (in the 6.5 to 6.7 A and 30 to 120 s range, respectively). The temperature was kept constant at 20 K for the duration of the experiments to maintain the most stable experimental conditions before, during, and between subsequent potassium evaporations.

AUTHOR INFORMATION

The authors declare no competing financial interests. Correspondence and requests for materials should be addressed to D. Fournier (dfournie@physics.ubc.ca) and A. Damascelli (damascelli@physics.ubc.ca).

SUPPLEMENTARY INFORMATION

Effective hole-doping determination

As discussed in the paper, the data presented in Fig. 1 and 2 (paper), consistent with the observed doping and the $T = 20$ K temperature of the experiments, reproduce the major features of the cuprate electronic structure in the overdoped normal metal ($p = 0.29$, $T > T_c$), the nearly-optimally doped superconductor ($p = 0.20$, $T < T_c$), and the underdoped pseudogap state ($p = 0.06$, $T_c < T < T^*$). Most importantly, they demonstrate that in situ potassium doping of the cleaved surface of YBCO is a very effective mean of exploring the whole cuprate phase diagram via surface-sensitive single-particle spectroscopies. To this end, a crucial aspect of the data analysis is the conversion from K-evaporation to the effective hole doping p per planar copper. If each K atom deposited on as-cleaved YBCO donates one electron to the surface electronic structure, the resulting K^{1+} ions should be more likely located on the insulating and charge-neutral BaO termination, rather than on the (1+)-charged CuO chain termination. This is confirmed

by our scanning tunneling microscopy (STM) study of various YBCO samples after K-evaporation, which consistently finds K atoms on BaO terminations only; this is shown in Fig. 4a for the case of ortho-II YBCO6.5. STM was performed at $10\,\mathrm{K}$ and $2.0\mathrm{x}10^{-11}$ torr with a beetle type STM, and the same SAES getter source and procedures used in the ARPES experiments; tungsten tips were cleaned in situ by Ar sputtering and sharpened through gentle contact with an Au surface. Topographic images on BaO (CuO chain) terminations were acquired with bias voltage and tunnelling current of $-200\,\mathrm{mV}$ and $200\mathrm{pA}$ ($-600\,\mathrm{mV}$ and $500\,\mathrm{pA}$). We studied a total of 10 samples of different bulk doping from the same batches as those used for ARPES.

With respect to the doping evolution of the top-most BaO, CuO-chain, and CuO$_2$-plane layers, the ansatz to be proven is that the electrons donated by potassium will be sufficiently delocalized to lead to a uniform carrier doping. In Fig. 4b we show, for various as-cleaved and lightly K-deposited samples, the binding energy of the BaO band (BE_{BaO}), as well as the volume (counting electrons) of CuO-chain and (bonding and antibonding) CuO$_2$-plane Fermi surfaces (FS_{Ch}, FS_B, and FS_{AB}). Note that, in this very overdoped regime in which all Fermi surfaces are well-defined, the effective hole doping p can be determined directly from the average volume of FS_B and FS_{AB}, with no ambiguity. Interestingly, the same quantities estimated from LDA calculations for fully oxygenated YBCO7, upon a rigid shift of the chemical potential, show good overall quantitative agreement suggesting that, beyond $\simeq 0.25$, the electronic structure is well described by independent-particle density-functional theory (for the BaO band, which LDA puts closer to the Fermi energy, the values in Fig. 4b were obtained by shifting it down *self-consistently* to match the BE observed for $p = 0.37$ as the extreme starting point). As we further hole-underdoped the system below $p \simeq 0.25$ by K-evaporation, we cannot rely on the volume of FS_B and FS_{AB} in determining p because of the opening of the superconducting gap and, eventually, the collapse of the CuO$_2$ Fermi surfaces into disconnected Fermi arcs. We can however follow very clearly the increase of the (electron) FS_{Ch} volume (Fig. 4e for YBCO7, sample 1) and of the BaO-band binding energy [Fig. 1d,f,h (paper), for various bulk dopings]. The results for all evaporation steps on YBCO7S1 are summarized in Fig. 4c, and demonstrate that both FS_{Ch} and BE_{BaO} scale linearly with the amount of deposited potassium, all the way to the highest surface doping. Similar scalings are observed for all bulk oxygen contents, leading to one universal linear scaling relation between ΔFS_{Ch} and ΔBE_{BaO}, for all YBCO samples (Fig. 4d). Note that the increase in both FS_{Ch} and BE_{BaO} upon K-evaporation (i.e., upward slopes in Fig. 4c,d) confirms once again the electron-nature of the doping induced by K (i.e., effective hole-underdoping). Furthermore, the linearity over the whole

doping range is consistent with the uncorrelated behaviour predicted for both BaO and CuO chain-derived electronic states in LDA+U calculations [11]. Quantitatively, the K-induced rate $\Delta BE_{BaO}/\Delta FS_{Ch} = 0.0323 \pm 0.0012\,[eV\,(\%BZ)^{-1}]$ obtained from Fig. 4d matches almost perfectly the ratio ~ 0.0331 obtained from the evolution of ΔBE_{BaO} and ΔFS_{Ch} versus hole doping p in both as-cleaved results and LDA calculations in Fig. 4b [here we observed $\Delta BE_{BaO}/p = 0.5059\,(eV\,p^{-1})$
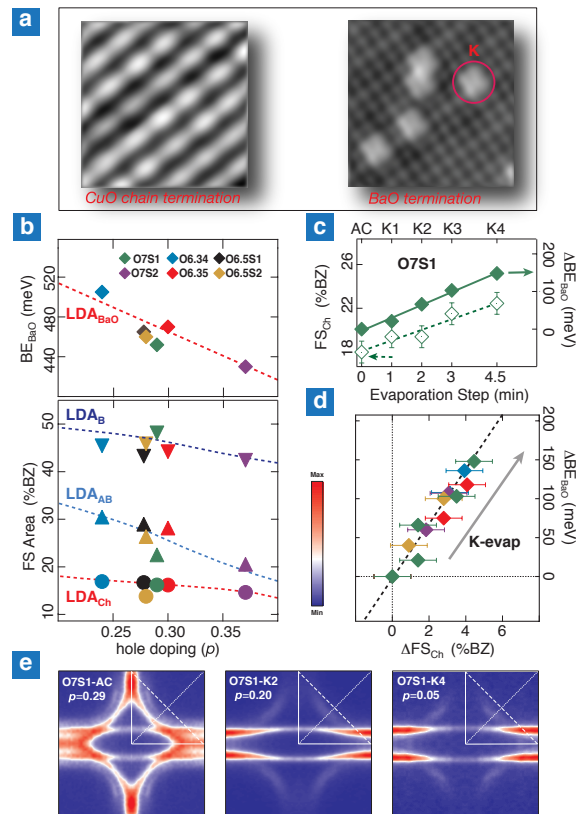
FIG. 4: **K-evaporation: effective hole-doping determination.** (a) Topographic STM images ($4\mathrm{x}4\,\mathrm{nm}^2$) from oxygen-ordered ortho-II YBCO6.5 confirm the approximately 50-50 % CuO-BaO termination of the cleaved surface, the ortho-II alternation of full and empty chains, and the preferential location on the BaO termination of evaporated K (red circle). (b) Binding energy of the BaO band (BE_{BaO}), and volume (counting electrons) of FS_{Ch}, FS_B, and FS_{AB}, plotted versus the hole doping p together with the results of LDA band-structure calculations [11]. In this very overdoped regime, in which all Fermi surfaces are well-defined on both as-cleaved and moderately K-deposited YBCO, the hole doping p is determined from the average volume of FS_B and FS_{AB} (symbols refer to different bulk oxygen contents). (c) Volume of FS_{Ch} and variation of the BaO binding energy (ΔBE_{BaO}) versus the K-evaporation time for YBCO7. (d) The relative evolution of ΔBE_{BaO} and ΔFS_{Ch} upon K-deposition is linear over the whole range for all samples. (e) Fermi surface mapping from as-cleaved and K-deposited YBCO7.

Structure/doping	Nodal bilayer splitting (eV)
Bulk YBCO$_{6.0}$	0.19
Bulk YBCO$_{6.5}$	0.21
Bulk YBCO$_{7.0}$	0.24
Slab YBCO$_{7.0}$	
BaO$_{surf}$	0.18
CuO$_{surf}$	0.23
Slab YBCO$_{7.0}$ with K	
BaO$_{surf}$	0.21
CuO$_{surf}$	0.19

TABLE I: Nodal bilayer splitting values for various YBCO bulk and surface structures, as obtained from WIEN2K density functional theory calculations for $k_z = 0$.

and $\Delta FS_{Ch}/p = 15.269\,(\%BZ\,p^{-1})$]. This provides a uniquely accurate measure of the charge carriers injected into the system upon K-evaporation, which can be expressed in terms of the usual hole doping parameter p, i.e. the number of holes per planar copper away from half filling ($p = 0$).

Electrostatic effects from oxygen and potassium doping

In the following we address the question of the sensitivity of bilayer splitting to doping and crystal structure for various oxygen concentrations in bulk YBCO, as well as to the electrostatic effects associated with different O^{2-} fillings in the CuO chain layers sandwiching a CuO$_2$ bilayer, or the presence of the surface either as-cleaved or potassium evaporated. All these configurations have been investigated by density functional theory (DFT) calculations using the linearized augmented-plane-wave method implemented in the WIEN2K code [34]; exchange and correlation effects were treated within the local-density approximation (LDA) [35]. As a further check, we have also done calculations using the DFT code SIESTA [36], with the norm-conserving Troullier-Martins pseudopotentials [37] and the double-ζ singly-polarized basis set; the exchange and correlation effects were again treated within LDA, after Ceperley and Alder [38]. The results obtained with the two methods are in very good agreement, with a $\lesssim 0.02\,\mathrm{eV}$ variation in bilayer splitting; the WIEN2K values are summarized in Tab. I.

The YBCO$_{6+x}$ band structure calculations, for $x = 1$ and 0, were performed using the crystal structures reported by Jorgensen *et al.* [39] for $x = 0.93$ and 0.09,

respectively. To study the effect of a non-symmetric potential on bilayer splitting in a direction parallel to the c-axis, we calculated the electronic structure of YBCO6.5 using an artificial layered structure consisting of alternating full and empty chain layers. As one can see in Tab. I, the bilayer splitting is only weakly dependent on doping. The influence on bilayer splitting of the surface termination, either of BaO or CuO chain type, can be estimated with YBCO7.0 slab calculations. We adopted an ideal bulk crystal structure and periodic slab geometry with 18 Å separation between the slabs. The slabs are 3 unit cells thick and stoichiometric, with BaO termination on one side and CuO chain termination on the another, which allows us to account for the effects associated with the polar catastrophe [40]. In the K-deposited YBCO7.0 slab calculations the K-position is relaxed, whereas the YBCO atomic positions are kept fixed according to the bulk structure; the computed distance between K and BaO (CuO chain) surface is 2.57 Å (2.5 Å). As shown in Tab. I, also for 'clean' and K-deposited BaO and CuO surface terminations we observe a negligible effect on the value of bilayer splitting. We can thus conclude that, within DFT, the CuO$_2$ bilayer band splitting is almost independent of the doping as well as the change in potential introduced by different filling of the CuO chain and the presence of the surface, whether as-cleaved or K evaporated. For the purpose of a more direct comparison with the existing literature, in the paper we will refer to the values of nodal and antinodal bilayer splitting $t_\perp^{LDA}(k)$ as obtained for YBCO7.0 in bulk calculations.

Nodal quasiparticle weight estimate

Formally, the degree of quasiparticle integrity is revealed by $Z_k \equiv \int A_{coh}(k,\omega)\,d\omega$, i.e. the integrated spectral weight of the coherent part of the single-particle spectral function probed by ARPES [16, 17]. Experimentally, while in the optimally-to-overdoped regime Z_k is believed to be finite – yet quantitatively undetermined – at all momenta both above and below T_c, the situation is much more controversial in the optimally-to-underdoped regime [16, 17]. In the following, as in the rest of the paper, we concentrate on the behaviour of the nodal quasiparticles because they are better defined over a larger portion of the phase diagram. In addition, since they are not affected by the opening of pseudo and superconducting gaps, they are not characterized by as dramatic a temperature dependence as the antinodal quasiparticles; they can therefore be studied at low temperatures, while still providing insights on the normal liquid underlying the emergence of HTSC. To illustrate the limitations even in the nodal region in the quantitative estimate of the quasiparticle integrity from the spectral weight of $A_{coh}(k,\omega)$ as measured by ARPES, we present a detailed analysis in Fig. 5. As shown in Fig. 5a, using YBCO6.34
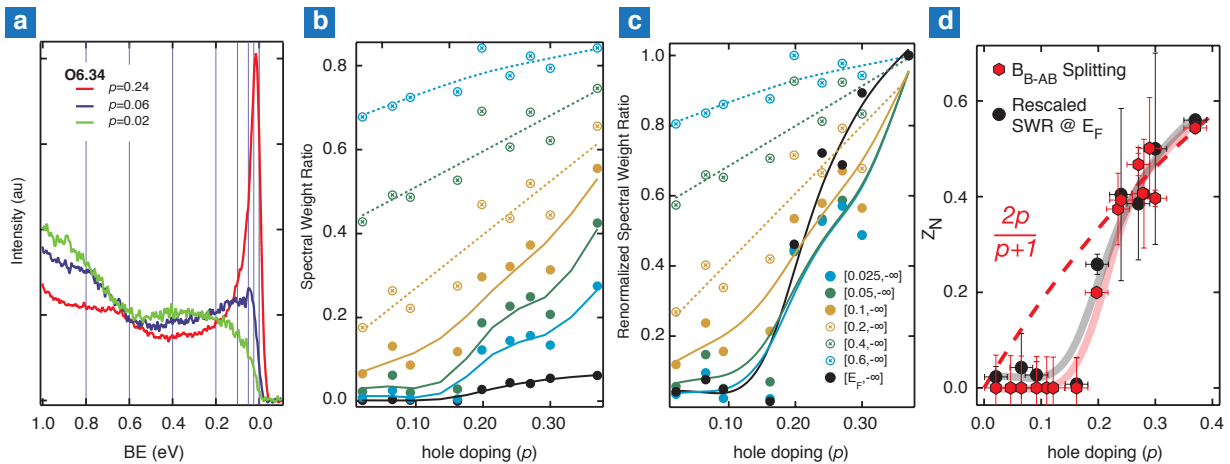
FIG. 5: **Nodal quasiparticle integrity from spectral weight ratios.** (a) ARPES spectra at the nodal Fermi wavevector $k_{F,N}$ from YBCO6.34. (b) Nodal spectral-weight ratio (SWR), defined as $\int_{BE_{min}}^{-\infty} I(k_{F,N}, \omega)\, d\omega / \int_{0.8\,eV}^{-\infty} I(k_{F,N}, \omega)\, d\omega$, where $I(k, \omega) = I_0(k) f(\omega) A(k, \omega)$ is the intensity measured by ARPES; the data are presented versus doping for progressively increasing integration windows (as indicated in c). In (c), the same SWRs are renormalized to the $p = 0.37$ value. (d) Nodal quasiparticle renormalization Z_N as determined from the observed bilayer splitting and the SWR estimated at E_F (the latter was rescaled so that the two curves match in the $0.23-0.37$ doping range), together with the mean-field relation $2p/(p+1)$ [13, 14]; thick gray and orange lines are guides to the eye. For the bilayer splitting data, the error bars are defined from the B-AB MDC fits when bilayer splitting is detected, and from the experimental resolutions otherwise; for the SWR data, they are calculated from the spread in the SWR values for integration windows smaller than $[0.1, -\infty]$ in binding energy (BE).

as an example, a clear peak is detected at large doping values, which loses intensity upon underdoping and eventually disappears. The first practical challenge in estimating $Z_k = \int A_{coh}(k, \omega)\, d\omega$ is that ARPES does not measure directly $A(k, \omega) \equiv A_{coh}(k, \omega) + A_{incoh}(k, \omega)$ but rather $I(k, \omega) = I_0(k) f(\omega) A(k, \omega)$. This is proportional to $A(k, \omega)$ via the Fermi-Dirac distribution function $f(\omega)$ and the one-electron dipole matrix-element $I_0(k)$, which however remains experimentally undetermined (this is the so-called 'matrix-element effect' that makes the absolute value of the photoemission signal a strong and generally unknown function of polarization, photon energy, and experimental geometry [16, 17]). To circumvent this problem, since the dipole matrix element is the same for both A_{coh} and A_{incoh}, one can try to evaluate experimentally $Z_k = \int I_{coh}(k, \omega)\, d\omega / \int I(k, \omega)\, d\omega$. This is precisely the strategy followed for instance in Ref. 21 and 22, which however leads to two additional challenges: (i) As already obvious from the data in Fig. 5a, I_{coh} is strongly dependent on doping and progressively more difficult to identify upon underdoping; a variety of phenomenological methods have been applied to estimate and remove the incoherent background from $I(k, \omega)$, either based on the fit of the background by ad-hoc polynomial, linear, and integral functions [21, 22], or on the estimate of the background from the spectral weight detected beyond k_F [24, 41] (i.e., from in principle unoccupied regions of momentum space). (ii) A_{incoh}, and thus the integral of the complete $A(k, \omega)$, extend over a large energy scale given by $U/2 \simeq 4\,eV$ [1, 11, 15]; they cannot be properly

quantified due to the overlap with other electronic states, such as oxygen bands starting already at 1-2 eV BE in all cuprates and, in YBCO in particular, also BaO and CuO chain bands. As a consequence, even if one could estimate $\int I_{coh}(k, \omega)\, d\omega$, an absolute quantitative value for Z_k would still be lacking due to $\int I(k, \omega)\, d\omega$.

To follow the evolution of the low-energy spectral weight versus doping, and attempt an heuristic distinction between its coherent and incoherent components, in Fig. 5b we plot the nodal spectral weight ratio (SWR) defined as $\int_{BE_{min}}^{-\infty} I(k_{F,N}, \omega)\, d\omega / \int_{0.8\,eV}^{-\infty} I(k_{F,N}, \omega)\, d\omega$, for various integration windows extending from above E_F ($-\infty$) to a finite binding energy below E_F (BE_{min}). Although the SWR is numerically dependent on the arbitrary choice of the full integration window ([0.8, $-\infty$] in this particular case to avoid the large contribution from the oxygen-related features), it is obvious that the narrower integration windows will capture more directly the degree of quasiparticle coherence. As one can see in Fig. 5b, and even more clearly in Fig. 5c where the SWR data have been renormalized to the $p = 0.37$ value, there is a large systematic dependence on the choice of the integration window. Although it is not possible to reach any quantitative conclusion based on such kind of data, a clear qualitative change occurs when the window extends beyond the 50 meV BE range: for $BE_{min} \leq 50\,meV$ the SWR consistently vanishes below $p \simeq 0.15$, while it becomes finite at all doping – and progressively larger – for wider integration windows (eventually approaching unity once BE_{min} gets closer to 0.8 eV). Since, as

shown in Fig. 5a, the sharpest component of the nodal spectra is located well within the first 50 meV across the whole phase diagram, it is natural to associate the low-energy SWR with a relative measure of the quasiparticle integrity Z_N; remarkably, the doping evolution of this low-energy SWR is also reminiscent of the quasiparticle renormalization inferred from the observed bilayer splitting through the relation $Z_N = \Delta\epsilon_N^{B,AB}/2t_\perp^{LDA}(N)$. When the two results are plotted together (after the necessary rescaling of the SWR, so that the two curves match in the $0.23-0.37$ doping range), the similarity is striking. This validates the quantitative determination of Z_N from the evolution of bilayer band splitting and confirms our conclusion of a rapid loss of nodal quasiparticle integrity in the $p \simeq 0.10-0.15$ doping range, possibly consistent with the results of cluster dynamical mean-field theory which predicts a rapid suppression of Z_N in this same doping range [15].

[1] M. B. J. Meinders, H. Eskes, and G. A. Sawatzky, Phys. Rev. B **48**, 3916 (1993).
[2] Y. Kohsaka, C. Taylor, K. Fujita, A. Schmidt, C. Lupien, T. Hanaguri, M. Azuma, M. Takano, H. Eisaki, H. Takagi, et al., Science **315**, 1380 (2007).
[3] D. C. Peets, D. G. Hawthorn, K. M. Shen, Y.-J. Kim, D. S. Ellis, H. Zhang, S. Komiya, Y. Ando, G. A. Sawatzky, R. Liang, et al., Phys. Rev. Lett. **103**, 087402 (2009).
[4] P. W. Anderson, Science **235**, 1196 (1987).
[5] N. Doiron-Leyraud, C. Proust, D. LeBoeuf, J. Levallois, J.-B. Bonnemaison, R. Liang, D. A. Bonn, W. N. Hardy, and L. Taillefer, Nature **447**, 565 (2007).
[6] S. E. Sebastian, N. Harrison, M. M. Altarawneh, R. Liang, D. A. Bonn, W. N. Hardy, and G. G. Lonzarich, arXiv:0912.3022 (2009).
[7] A. Comanac, L. de Medici, M. Capone, and A. J. Millis, Nature Phys. **4**, 287 (2008).
[8] S. Sachdev, arXiv:0907.0008 (2009).
[9] M. A. Hossain, J. D. F. Mottershead, D. Fournier, A. Bostwick, J. L. McChesney, E. Rotenberg, R. Liang, W. N. Hardy, G. A. Sawatzky, I. S. Elfimov, et al., Nature Phys. **4**, 527 (2008).
[10] O. Andersen, A. Liechtenstein, O. Jepsen, and F. Paulsen, J. Phys. Chem. Solids **56**, 1573 (1995).
[11] I. S. Elfimov, G. A. Sawatzky, and A. Damascelli, Phys. Rev. B **77**, 060504(R) (2008).
[12] K. Pasanai and W. A. Atkinson, Phys. Rev. B **81**, 134501 (2010).
[13] P. W. Anderson, P. A. Lee, M. Randeria, T. M. Rice, N. Trivedi, and F. C. Zhang, J. Phys.: Condens. Matter **16**, R755 (2004).
[14] K. Y. Yang, T. M. Rice, and F. C. Zhang, Phys. Rev. B **73**, 174501 (2006).
[15] K. Haule and G. Kotliar, Phys. Rev. B **76**, 104509 (2007).
[16] A. Damascelli, Z. Hussain, and Z.-X. Shen, Rev. Mod. Phys. **75**, 473 (2003).
[17] J. Campuzano, M. Norman, and M. Randeria, *Photoemission in the High T_c Superconductors* (Springer, Berlin, 2004), vol. II, pp. 167–265.
[18] A. Kanigel, M. R. Norman, M. Randeria, U. Chatterjee, S. Souma, A. Kaminski, H. M. Fretwell, S. Rosenkranz, M. Shi, T. Sato, et al., Nature Phys. **2**, 447 (2006).
[19] U. Chatterjee, M. Shi, D. Ai, J. Zhao, A. Kanigel, S. Rosenkranz, H. Raffy, Z. Z. Li, K. Kadowaki, D. Hinks, et al., Nature Phys. **6**, 99 (2010).
[20] Z.-X. Shen and G. A. Sawatzky, Phys. Stat. Sol. B **215**, 523 (1999).
[21] D. L. Feng, D. H. Lu, K. M. Shen, C. Kim, H. Eisaki, A. Damascelli, R. Yoshizaki, J.-i. Shimoyama, K. Kishio, G. Gu, et al., Science **289**, 277 (2000).
[22] H. Ding, J. R. Engelbrecht, Z. Wang, J. C. Campuzano, S.-C. Wang, H.-B. Yang, R. Rogan, T. Takahashi, K. Kadowaki, and D. G. Hinks, Phys. Rev. Lett. **87**, 227001 (2001).
[23] A. Kaminski, S. Rosenkranz, H. M. Fretwell, Z. Z. Li, H. Raffy, M. Randeria, M. R. Norman, and J. C. Campuzano, Phys. Rev. Lett. **90**, 207003 (2003).
[24] M. Platé, J. Mottershead, I. Elfimov, D. Peets, R. Liang, D. Bonn, W. Hardy, S. Chiuzbaian, M. Falub, M. Shi, et al., Phys. Rev. Lett. **95**, 159 (2005).
[25] H. Lin, S. Sahrakorpi, R. S. Markiewicz, and A. Bansil, Phys. Rev. Lett. **96**, 097001 (2006).
[26] K. M. Shen, F. Ronning, D. H. Lu, F. Baumberger, N. J. C. Ingle, W. S. Lee, W. Meevasana, Y. Kohsaka, M. Azuma, M. Takano, et al., Science **307**, 901 (2005).
[27] W. S. Lee, I. M. Vishik, K. Tanaka, D. H. Lu, T. Sasagawa, N. Nagaosa, T. P. Devereaux, Z. Hussain, and Z.-X. Shen, Nature **450**, 81 (2007).
[28] J. Graf, G.-H. Gweon, K. McElroy, S. Zhou, C. Jozwiak, E. Rotenberg, A. Bill, T. Sasagawa, H. Eisaki, S. Uchida, et al., Phys. Rev. Lett. **98**, 067004 (2007).
[29] S. Hüfner, M. A. Hossain, A. Damascelli, and G. A. Sawatzky, Rep. Prog. Phys. **71**, 062501 (2008).
[30] A. Dubroka, D. Munzar *et al.* (2010).
[31] I. Dimov, P. Goswami, X. Jia, and S. Chakravarty, Phys. Rev. B **78**, 157003 (2008).
[32] A. Audouard, C. Jaudet, D. Vignolles, R. Liang, D. Bonn, W. Hardy, L. Taillefer, and C. Proust, Phys. Rev. Lett. **103**, 157003 (2009).
[33] Y. S. Lee, K. Segawa, Z. Q. Li, W. J. Padilla, M. Dumm, S. V. Dordevic, C. C. Homes, Y. Ando, and D. N. Basov, Phys. Rev. B **72**, 054529 (2005).
[34] P. Blaha, K. Schwarz, G. Madsen, D. Kvasnicka, and J. Luitz, WIEN2K, ISBN 3-9501031-1-2 (TU Wien, Austria, 2001).
[35] J. Perdew and Y. Wang, Phys. Rev. B **45**, 13244 (1992).
[36] J. M. Soler, E. Artacho, J. D. Gale, A. García, J. Junquera, P. Ordejón, and D. Sánchez-Portal, J. Phys.: Condens. Matter **14**, 2745 (2002).
[37] N. Troullier and J. Martins, Phys. Rev. B **43**, 1993 (1991).
[38] D. Ceperley and B. Alder, Phys. Rev. Lett. **45**, 566 (1980).
[39] J. D. Jorgensen, B. W. Veal, A. P. Paulikas, L. J. Nowicki, G. W. Crabtree, H. Claus, and W. K. Kwok, Phys. Rev. B **41**, 1863 (1990).
[40] X. Gu, I. Elfimov, and G. Sawatzky, arXiv:0911.4145 (2009).
[41] A. Kaminski, S. Rosenkranz, H. M. Fretwell, J. Mesot, M. Randeria, J. C. Campuzano, M. R. Norman, Z. Z. Li, H. Raffy, T. Sato, et al., Phys. Rev. B **69**, 212509 (2004).